

Real-Time Prediction of Structural Processes with Polymorphic Uncertain Data

Ba Trung Cao, Steffen Freitag and Günther Meschke

Institute for Structural Mechanics, Ruhr University Bochum, Universitätsstr. 150, 44801, Bochum, Germany, ba.cao@rub.de, steffen.freitag@sd.rub.de, guenther.meschke@rub.de

Abstract: The focus of this paper is on the development and comparison of two interval approaches for real-time predictions of high dimensional structural processes, i.e. the prediction of uncertain time variant displacement fields of a structure due to a few steering parameters. The approaches are developed for simulation supported steering of mechanized tunneling processes but can also be applied to similar problems in structural mechanics. Using interval data for uncertainty quantification in mechanized tunneling is motivated by the geotechnical reports of tunnel projects, where often ranges for the geotechnical data (dimension of soil layers) and some soil parameters (e.g. modulus of elasticity, friction angle) are provided. For real-time simulations with interval data, two surrogate modeling strategies (Proper Orthogonal Decomposition and Artificial Neural Networks) are combined to substitute the structural simulation model, which is in the presented application a process oriented 3D finite element (FE) model for shield tunneling taking into account all relevant components of the construction process. The hybrid surrogate model is trained in the offline (design) stage with patterns of interval data obtained with an optimization based interval analysis. However, this approach is time consuming and not suitable for real-time predictions of high dimensional output data, e.g. nodal displacements of a FE model. For real-time steering in the online (construction) stage, the optimization based interval analysis is replaced by a direct prediction with interval data using either midpoint-radius representation or lower-upper-bound representation of intervals. Both approaches are presented in the paper and compared within a verification example and an application example in mechanized tunneling. It is also demonstrated, how these new surrogate modeling approaches for time variant interval fields can be applied in case of polymorphic uncertain data (combination of interval and stochastic parameters) within the probability-box (p-box) approach using interval Monte Carlo Simulation.

Keywords: surrogate models, real-time prediction, interval, probability box, finite element analysis

1. Introduction

Mechanized tunneling in urban areas must always consider the effect of the construction process on the built environment, e.g. the risk of damage of existing buildings or infrastructure on the surface. Currently, FE simulations are more commonly used in a deterministic framework to investigate and predict the structural behavior in mechanized tunneling processes. For reliability analyses taking the uncertainty of geotechnical parameters into account, multiple runs of the simulation model are required, at least a few hundreds within optimization approaches for interval or fuzzy analyses or

up to 10^6 within Monte Carlo simulations, e.g., to predict failure probabilities. Hence surrogate models are required to replace the FE simulation models with the aim to maintain the prediction performance and to reduce the computation time significantly, especially for real-time applications.

Recently, in (Freitag et al., 2015), reliability analyses approaches in mechanized tunneling were presented, taking polymorphic uncertain geotechnical data by means of stochastic numbers, intervals and interval stochastic numbers into account. The analyses are performed with a hybrid surrogate model (i.e. a combination of Proper Orthogonal Decomposition (POD) and Recurrent Neural Networks (RNN)), for deterministic input-output mappings within optimization based interval analyses and interval stochastic analyses using Particle Swarm Optimization (PSO). The hybrid surrogate model has the capability to predict (extrapolate) tunneling induced uncertain time and spatially varying surface settlements, see also (Cao et al., 2016). Based on the RNN predictions at selected monitoring points of the settlement field, the Gappy POD (GPOD) method is utilized to approximate the complete surface settlement field. The optimization based interval analysis approach is useful for reliability assessment in the design stage of a project, because the computational time is between one and several hours using a standard laptop and increases dramatically especially for a large number of outputs (e.g. settlements at all surface points). This is because of the fact, that for each output two separate optimization problems have to be solved to compute the corresponding lower and upper interval bounds.

In order to support the steering of the tunnel boring machine (TBM) during the tunnel construction, the computation time of optimization based approaches may be inappropriate since the computational time needs to be significantly smaller than the time required for one tunnel ring construction stage, which is typically in the range between 2-4 hours. Therefore, a real-time prediction should be performed in the ranges of seconds to some minutes to investigate the influence of the steering parameters onto the outputs, e.g. surface settlements. This can be achieved by solving the independent optimization tasks for each output in parallel, e.g. using a computer cluster or by direct interval computations. Here, two interval computation approaches are presented.

The first approach is based on the midpoint-radius representation and is described in detail in (Freitag et al., 2016). The idea is to develop separate surrogate models for predicting the midpoints and the radiuses of the intervals. For the midpoints, the approach is identical to (Freitag et al., 2015). Meanwhile, the radiuses are restricted to positive numbers. This is satisfied by selecting activation functions with only positive outputs in the RNN part and by applying the Non-Negative Matrix Factorization (NNMF) in the GPOD part of the hybrid surrogate model.

The second approach is based on the lower-upper bound representation of intervals. Whereas the computation of the interval bounds with RNNs using interval arithmetic can directly be adopted from (Freitag et al., 2011) (RNNs for fuzzy data), two separate surrogate models for the lower and upper bound predictions are developed for the GPOD part, respectively. First, the upper bounds are computed with the same approach as presented in (Freitag et al., 2015). But for the lower bounds prediction, a constraint, not to exceed the upper bound, is defined within the GPOD approach.

The structure of this paper is organized as follows. Section 2 provides a short overview of the process-oriented FE model for numerical simulations of mechanized tunneling processes. Polymorphic uncertain data models are introduced in Section 3. In Section 4, the concept of the hybrid surrogate modeling strategy for time variant interval fields in mechanized tunneling is explained. Consequently, Section 5 presents how interval data are processed with the surrogate model. The

verification and comparison of the two approaches with an analytical solution and an application example are finally shown in Section 6.

2. Numerical Simulation of Mechanized Tunneling Processes

A process-oriented, three-dimensional, FE model is applied to simulate the tunneling process. The simulation model is based on (Kasper and Meschke, 2004) and has been further developed to the simulation model `ekate`, see e.g. (Nagel et al., 2010), using a more advanced and flexible software architecture within the object-oriented FE framework KRATOS. All relevant components involved in the mechanized tunneling process are considered, i.e. the soil layers, existing structures, the shield machine, the segmented lining, the face support, and the tail void grouting. The FE model follows the tunneling construction stages during the numerical simulation, see also (Meschke et al., 2013).

The soil is modeled as a three or two phase material for partially or fully saturated soils respectively, see (Nagel and Meschke, 2010). A surface-to-surface contact algorithm (Laursen, 2002), which allows for a smooth advancement of the machine is employed to simulate the movement of the TBM through the soil. Face support and grouting pressures are applied to ensure the stability of the tunnel face due to distortions caused by the excavation process and to reduce ground loss behind the tapered shield, respectively. The tail void grout is described as a fully saturated two-phase material considering hydration-dependent material properties of the cementitious grouting material as proposed in (Meschke, 1996). This formulation allows to model the infiltration of fluid grout into the surrounding soil. After each TBM advance, the excavation at the cutting face, the tail void grouting and the erection of a new lining ring during standstill are taken into account by deactivation of soil elements and adjusting all boundary conditions to the new situation. The effect of existing structures at the surface is accounted by adopting substitute models with equivalent thickness and stiffness. In (Ninić, 2015), the model has been employed to perform in-depth investigations of soil-structure interactions during mechanized tunneling processes.

3. Polymorphic Uncertain Data

Polymorphic uncertainty modeling allows to combine several uncertainty concepts to consider aleatoric and epistemic sources of uncertainties within one numerical simulation, see e.g. (Graf et al., 2014). The input space can be a combination of intervals, fuzzy numbers and stochastic numbers (i.e. each input parameter is described by diverse uncertainty models), or some input parameters are polymorphic uncertain itself, e.g. defined as p-boxes or fuzzy stochastic numbers. Both situations of polymorphic uncertain input parameters can be treated in a similar way within numerical simulations and require to combine stochastic and non-stochastic simulation approaches and finally lead to imprecise stochastic responses (outputs), e.g. p-boxes, fuzzy stochastic numbers, interval or fuzzy failure probabilities. In this paper, it is focused on real-time simulations with interval data and its possible application within the p-box approach.

3.1. INTERVALS

Geotechnical parameters with epistemic sources of uncertainty can be quantified by intervals or fuzzy numbers. Here, it is focused on intervals

$$\bar{x} = [{}_l x, {}_u x] , \quad (1)$$

which are ranges with lower bounds ${}_l x$ and upper bounds ${}_u x$. The intervals can directly be obtained from geotechnical reports, which often contain possible ranges for the expected geotechnical parameters. An alternative to the lower-upper bound representation of intervals is the midpoint-radius representation, where the midpoint ${}_m x$ and radius ${}_r x$ of an interval \bar{x} is defined as

$${}_m x = \frac{{}_l x + {}_u x}{2} \quad (2)$$

and

$${}_r x = \frac{{}_u x - {}_l x}{2} . \quad (3)$$

Interval arithmetic (Moore., 1979), the transformation method (Hanss, 2002), or optimization approaches, see e.g. (Möller et al., 2000), can be utilized to compute with intervals. The interval finite element method (IFEM) (Muhanna et al., 2007; Rao et al., 2011) has been developed for applications in structural mechanics, see also (Moens and Vandepitte, 2005; Moens and Hanss, 2011) for an overview.

3.2. PROBABILITY BOXES

The probability box (p-box) approach, see e.g. (Ferson et al., 2003), allows to define imprecise stochastic numbers by a lower bound ${}_l F(x)$ and an upper bound ${}_u F(x)$ cumulative distribution function (cdf). In general, arbitrary stochastic models, including empirical distributions, can be used for the lower and upper bound cdf. Each distribution, which is inside the p-box is valid.

3.3. COMPUTING WITH INTERVALS AND STOCHASTIC NUMBERS

In order to compute with inputs defined as intervals and stochastic numbers, a combination of stochastic and interval analysis is required. This can be performed by a stochastic analysis with interval samples, e.g. by means of Interval Monte Carlo Simulation (Zhang et al., 2010). For each interval sample, the structural response has to be computed by optimization-based interval analysis or by approaches based on interval arithmetic, such as IFEM. In (Freitag et al., 2013), a surrogate modeling approach based on artificial neural networks is presented, which is applied to replace a time consuming optimization-based FE interval analysis within an Interval Monte Carlo Simulation to compute p-boxes of structural responses and also fuzzy failure probabilities. This idea is extended to a hybrid surrogate modeling approach for real-time surface settlement field predictions in mechanized tunneling.

4. Hybrid Surrogate Modeling Approach

During the tunnel advancement process, it is required to predict the surface settlement field in real-time to support the decision of choosing appropriate operational parameters such as grouting and support pressures. In (Freitag et al., 2015), a surrogate modeling strategy combining POD and RNN approaches is proposed to predict time-variant high-dimensional outputs (surface settlement fields) in mechanized tunneling. This hybrid surrogate model, which has been developed for deterministic real-time input-output mappings in (Cao et al., 2016), is extended for predictions with interval data in this paper. In Table I the proposed surrogate modeling strategy for interval data is summarized.

Table I. Hybrid surrogate modeling approach to predict time-variant interval settlement fields.

Offline stage
1: Create a numerical model representing a tunnel section
2: Define intervals for geotechnical parameters $\bar{\mathbf{X}}$ and scenarios for deterministic steering parameters $^{[n]}\mathbf{P}$
3: Run numerical simulations with different realizations of input parameters
4: Store the numerical results of the deterministic settlement fields
5: Define intervals of the geotechnical parameter $\bar{\mathbf{X}}$
6: Perform interval analysis (optimization approach) for different patterns of $\bar{\mathbf{X}}$ and scenarios of deterministic steering parameters $^{[n]}\mathbf{P}$ using the deterministic surrogate model
7: Store the lower and upper bounds of the interval settlement fields
8: Provide the interval settlement data of several monitoring points for RNN training and testing
9: Provide the interval settlement data of the complete settlement field for POD-RBF training and testing
Online stage
1: Input: an interval of the geotechnical parameters, the recorded history from time steps 1 to N of the steering parameters and chosen values of steering parameters in the next time step $N + 1$
2: Approximate the bounds of the complete displacement field from time step 1 to N (by POD-RBF)
3: Predict the bounds of the interval settlements at selected points for next time step $N + 1$ (by RNN)
4: Predict the interval settlement field of next time step $N + 1$ (by GPOD)
5: Update the interval bounds of the complete settlement field from time step 1 to $N + 1$
6: Repeat steps 3 and 4 with updated values

In the offline stage, i.e. in the design stage of a tunnel project, deterministic input-output data sets are collected by varying the input parameters of the numerical model `ekate` used to represent the mechanized tunneling process within a tunnel section. The data sets are utilized to generate a surrogate model with deterministic inputs (geotechnical parameters \mathbf{X} , time-variant steering parameters $\mathbf{P}(t)$) and deterministic outputs (time-variant surface settlements $\mathbf{S}(t)$). To capture the uncertainty of geotechnical parameters by means of intervals $\bar{\mathbf{X}}$, the next step is to compute the corresponding system outputs in the context of an interval analysis. This is accomplished by employing the just-built deterministic surrogate model together with an optimization approach (e.g. PSO). The obtained results are patterns of interval $\bar{\mathbf{X}}$ and deterministic $\mathbf{P}(t)$ input data and the corresponding interval output data $\bar{\mathbf{S}}(t)$.

In the online stage, i.e. during the tunnel construction, the interval bounds of expected surface settlements have to be predicted by the surrogate model. For the prediction, the history of the operational parameters is adopted for the time steps 1 to N and the interval settlement field is computed based on chosen values of the steering parameters in time step $N + 1$. The complete settlement field from time step 1 to N is approximated by trained POD-RBF networks for the midpoints and the radiuses, respectively. For the predictions of several monitoring points at time step $N + 1$, trained RNNs are employed for midpoints and radiuses (midpoint-radius representation) or upper and lower bounds (upper-lower-bounds representation). Finally, reconstruction data techniques are applied to approximate the complete interval settlement field based on the outputs of the two previous methods. For midpoint-radius representation, the GPOD and NNMF approaches are adopted for the midpoints and the radiuses respectively. Meanwhile, upper bounds and lower bounds of the surface settlement field are reconstructed to satisfy the constraint of generating valid interval data by a constrained GPOD method. Finally, the predicted results are included into the available data set and the procedure is repeated for the subsequent steps.

5. Processing Interval Data with the Hybrid Surrogate Model

This section briefly describes the computational approaches of each component of the hybrid surrogate model for interval data: process prediction (prediction the settlements of selected monitoring points for the next time steps), field approximation by interpolating with complete data (approximation of the settlement fields from starting time step up to current time step) and reconstruction missing data (prediction of complete settlement field for the next time step).

5.1. PROCESS PREDICTION WITH RECURRENT NEURAL NETWORKS FOR INTERVAL DATA

For the approximation and prediction of dependencies between structural processes, recurrent neural networks (RNNs) are beneficial. RNNs are able to learn dependencies between data series without considering time as additional input parameter. This enables to capture time-dependent phenomena in data series and predict (extrapolate) further structural responses. The layered network structure of the RNNs is similar to the architecture of feed forward neural networks, see e.g. (Freitag, 2015). In addition to the hidden neurons, so-called context neurons are used to consider the structural history. For each hidden and each output neuron, a context neuron is assigned. These context neurons send time delayed context signals to the hidden and output neurons.

In order to process interval data with RNNs, optimization approaches or interval analysis can be applied, see e.g. (Freitag et al., 2011) to directly compute the lower and upper bounds by interval arithmetic operations, see also (Freitag, 2010). An alternative to these approaches is the midpoint-radius representation of interval data, where two separate RNNs for the midpoints and the radiuses are generated, see (Freitag et al., 2016).

Table II. POD procedure to find the basis vectors capture a desired accuracy.

Input: Given matrix \mathbf{S} , desired accuracy E
Output: Truncated POD basis vectors $\hat{\Phi}$
1: Compute covariance matrix $\mathbf{C} = \mathbf{S}^T \cdot \mathbf{S}$
2: Compute eigenvalue decomposition $[\Psi, \Lambda] = eig(\mathbf{C})$
3: Set $\Phi_i = \mathbf{S} \cdot \Psi_{-,i} / \sqrt{\lambda_i}$, where $\Psi_{-,i}$ is the i th column of matrix Ψ
4: Set $\lambda_i = \Lambda_{ii}$ for $i = 1, \dots, M$
5: Define K based on desired accuracy E as following $\sum_{i=1}^K \lambda_i / \sum_{i=1}^M \lambda_i \geq E$
6: return truncated POD basis $\hat{\Phi}$ by taking the first K columns of Φ

5.2. FIELD APPROXIMATION WITH COMPLETE INTERVAL DATA

In general, interval data can be split using midpoint-radius or lower-upper-bounds representations. If the latter is adopted, constraints are required to ensure that the prediction results for lower bound are always smaller than the results for upper bounds. Meanwhile, the first representation requires that the prediction for the radius component must be non-negative. In the paper, two separate POD-RBF surrogate models for the midpoints and the radiuses are created to produce quick predictions of the system response (i.e. the interval settlement field) corresponding to an arbitrary set of input parameters (realisations of geotechnical interval parameters and deterministic steering parameters) by interpolation between the sample data points. The basis idea of the POD approach and how to combine the method with RBF to form a surrogate model are described in detail in (Freitag et al., 2015). The below sections explain this procedure briefly.

5.2.1. Proper Orthogonal Decomposition

POD can be seen as a model reduction technique or as a widely used method in exploratory data analysis. This approach aims to extract a compact representation of high-dimensional data by projecting the data into a lower-dimensional space. The full orthonormal basis of the subspace can be used to approximate the given set of data in an optimal least-squares sense. By truncating the basis, cheap reduced order models or surrogate models are formed. POD approach has been known under various name depending on the area of application such as: Karhunen-Loeve Decomposition (KLD) (Karhunen., 1946; Loeve., 1978) in stochastics, Principal Component Analysis (PCA) in data analysis (Hotelling., 1933) or empirical orthogonal function in oceanography and meteorology (Lorenz, 1956). The procedure is explained in the algorithm in Table II.

A high-dimensional matrix \mathbf{S} and a single column of \mathbf{S} can be approximated as a linear combination of the truncated basis vectors $\hat{\Phi}$ as $\mathbf{S} \approx \hat{\Phi} \cdot \hat{\mathbf{A}}$ and $\mathbf{S}_i \approx \hat{\Phi} \cdot \hat{\mathbf{A}}_i$. At this step, *truncated* “amplitude” matrix and vector, $\hat{\mathbf{A}}$ and $\hat{\mathbf{A}}_i$, contain constant values associated with the given matrix \mathbf{S} . Hence, only an approximation for snapshots that were generated in the original high-dimensional snapshots matrix \mathbf{S} is available.

Table III. POD-RBF procedure to predict output system response from an arbitrary set of input parameters.

Input: Snapshots output matrix \mathbf{S} , snapshots input matrix \mathbf{z} , arbitrary input vector \mathbf{z}^* , desired accuracy E
Output: System response vector \mathbf{S}^*
1: Compute truncated POD basis $\hat{\Phi}$ based on E (see algorithm in Table II)
2: Compute $f_j(\mathbf{z}^i)$ with $\mathbf{z}^i = \mathbf{z}^*$ and $i, j = 1, \dots, M$
3: Form matrix \mathbf{F} from previous step
4: Compute $\hat{\mathbf{A}} = \hat{\Phi}^T \cdot \mathbf{S}$
5: Compute \mathbf{B} based on \mathbf{F} , $\hat{\mathbf{A}}$
6: Compute $f_j(\mathbf{z}^*)$ with $j = 1, \dots, M$
7: Form vector \mathbf{F}^* from previous step
8: return System response vector $\mathbf{S}^* = \hat{\Phi} \cdot \mathbf{B} \cdot \mathbf{F}^*$

5.2.2. POD-RBF

To pass from discrete type of a response to a rather continuous one, each amplitude vector is modified as a nonlinear function of input parameters on which the system depends. The amplitude matrix $\hat{\mathbf{A}}$ can be related to interpolation functions by an unknown matrix of constant coefficients \mathbf{B} .

$$\hat{\mathbf{A}} = \mathbf{B} \cdot \mathbf{F}, \quad (4)$$

\mathbf{F} , being a set of predefined interpolation functions $f_j(\mathbf{z})$ of input parameters \mathbf{z} , is given in the following form $\mathbf{F}_i = [f_1(\mathbf{z}^i) \dots f_j(\mathbf{z}^i) \dots f_M(\mathbf{z}^i)]^T$. The choice of $f_j(\mathbf{z})$ can be arbitrary and in this study inverse multiquadric radial function, a type of RBF (see (Hardy, 1990) for a description), is chosen as interpolation functions. An approximation of the output system response corresponding to an arbitrary set of input parameters is obtained following the algorithm in Table III.

5.3. RECONSTRUCTION INTERVAL MISSING DATA

5.3.1. Midpoint-radius representation

For midpoint-radius representation, the missing midpoints are reconstructed by the unconstrained GPOD and the NNMF approach is employed for the missing radiuses.

5.3.1.1. *Unconstrained GPOD* Another extension of POD based on a combination of basic POD method with linear regression is called Gappy POD (GPOD). The method has been developed in (Everson and Sirovich, 1995) to reconstruct human face images from incomplete data sets. The complete vector for the entire grid is reconstructed by combining POD basis together with gappy data (which is data given at very few of the grid points). Since there is no requirements for the outputs of the method, it is referred to "unconstrained GPOD" method in this paper. In (Bui-Thanh et al., 2004), this methodology was successfully employed for data reconstruction in the field of aerodynamic. The paper shows a very effective way to reconstruct the flowfields from incomplete aerodynamic data set by using GPOD. The gappy POD procedure is described below.

Without any missing data, an arbitrary snapshot \mathbf{S}_j , which belongs to a set of snapshots, can be approximated as a linear combination of the first K POD basis vectors $\hat{\Phi}$ and an amplitude vector $\hat{\mathbf{A}}_j$ as described in subsection "Proper Orthogonal Decomposition". The amplitude vector is calculated by minimising the error norm

$$\min. \|\mathbf{S}_j - \hat{\Phi} \cdot \hat{\mathbf{A}}_j\|_{L^2}^2 \quad (5)$$

The same least square approach can be effectively used to restore missing data of an incomplete data snapshot \mathbf{S}^* by

$$\min. \|\mathbf{S}^* - \hat{\Phi} \cdot \hat{\mathbf{A}}^*\|_{L^2}^2 \quad (6)$$

However, due to missing elements, the L^2 norm in Eq. (6) cannot be evaluated correctly. As a remedy, the Gappy POD procedure employs the concept of a gappy norm based on available data. Firstly, the locations of missing data must be identified by a vector \mathbf{m} as following

$$\begin{aligned} \mathbf{m}_i &= 0, & \text{for locations of unknown or missing data} \\ \mathbf{m}_i &= 1, & \text{for locations of known data} \end{aligned} \quad (7)$$

The gappy norm is defined with a gappy inner product $(\cdot, \cdot)_n$, such that

$$\|\mathbf{S}_j\|_n^2 = (\mathbf{S}_j, \mathbf{S}_j)_n = (m \circ \mathbf{S}^*, m \circ \mathbf{S}^*)_{L^2} = \|m \circ \mathbf{S}^*\|_{L^2}^2, \quad (8)$$

where \circ denotes point-wise multiplication. The complete (repaired) vector from \mathbf{S}^* can be reproduced using the assumption that \mathbf{S}^* can be characterized with the existing snapshots set \mathbf{S} . The intermediate repaired vector $\tilde{\mathbf{S}}^*$ can be expressed in terms of *truncated* POD basis vectors $\hat{\Phi}$ as follows

$$\tilde{\mathbf{S}}^* \approx \hat{\Phi} \cdot \hat{\mathbf{A}}^*. \quad (9)$$

The vector $\hat{\mathbf{A}}^*$ can be computed by minimizing the error $E = \|\mathbf{S}^* - \tilde{\mathbf{S}}^*\|_n^2$. A solution to this so-called *least squares* or *linear regression* problem is given by a linear system of equations

$$\mathbf{M} \cdot \hat{\mathbf{A}}^* = \mathbf{R} \quad (10)$$

with

$$\begin{aligned} \mathbf{M} &= (\hat{\Phi}^T, \hat{\Phi}) \\ \mathbf{R} &= (\hat{\Phi}^T, \mathbf{S}^*) \end{aligned} \quad (11)$$

Solving Eq. (9) with $\hat{\mathbf{A}}^*$ computed from Eqs. (10) and (11), the intermediate repaired vector $\tilde{\mathbf{S}}^*$ is obtained. Finally, by replacing the missing elements in \mathbf{S}^* by these in $\tilde{\mathbf{S}}^*$ the complete vector of output system responses is reconstructed. The step by step of GPOD procedure is shown in the algorithm in Table IV.

5.3.1.2. Non-Negative Matrix Factorization For midpoint-radius representation of interval data, the midpoint component is handled well with the unconstrained GPOD method described in previous section. Alternatively, the Non-Negative Matrix Factorization (NNMF) is utilized to ensure the

Table IV. GPOD procedure to reconstruct the complete solution vector from incomplete solution vector.

Input: Snapshots output matrix \mathbf{S} , mask vector \mathbf{m} , incomplete solution vector \mathbf{S}^* , desired accuracy E
Output: Complete solution vector \mathbf{S}^*
1: Compute truncated POD basis $\hat{\Phi}$ based on E (see algorithm in Tabel II)
2: Compute $\mathbf{M} = (\hat{\Phi}^T, \hat{\Phi})$
3: Compute $\mathbf{R} = (\hat{\Phi}^T, \mathbf{S}^*)$
4: Compute $\hat{\mathbf{A}}^*$ from \mathbf{M} and \mathbf{R}
5: Compute $\tilde{\mathbf{S}}^* = \hat{\Phi} \cdot \hat{\mathbf{A}}^*$
6: return Complete solution vector \mathbf{S}^* by replacing missing elements from corresponding elements of $\tilde{\mathbf{S}}^*$

positive sign of the reconstructed results for the radiuses. The NNMF was first suggested by Paatero and Tapper (Paatero and Tapper, 1994) as a concept of Positive Matrix Factorisation concentrating on a specific application concerned with Byzantine algorithms. Modern NNMF algorithms can be divided into four categories: Standard NNMF, Constrained NNMF, Structured NNMF and Generalised NNMF. In this paper, the Standard NNMF is utilized for radius predictions as described below.

Given a $(N \times M)$ non-negative matrix ${}_r\mathbf{S}$ and a reduced rank k , the NNMF algorithm is searching for two non-negative matrices $\mathbf{W}_{n \times k}$ and $\mathbf{H}_{k \times m}$ that satisfies the following optimization problem

$$\min. \frac{1}{2} \| {}_r\mathbf{S} - \mathbf{W} \cdot \mathbf{H} \|_F^2 \text{ subject to, } \mathbf{W}, \mathbf{H} \geq 0. \quad (12)$$

Similar to the POD approach, \mathbf{W} and \mathbf{H} are denoted as the *basis matrix* and *coefficient matrix*, respectively. The alternating non-negative least squares (NNLS) algorithm proposed in (Kim and Park., 2008), which ensures the convergence of the minimization problem in Eq. (12), is implemented in this paper.

The reconstruction procedure for a non-negative vector containing the radiuses \mathbf{S}^+ now can follow the steps listed in the GPOD method with some minor modifications. The corresponding objective function $\mathbf{E} = \| \mathbf{S}^+ - \mathbf{W} \cdot \mathbf{H}^+ \|_n^2$ to be minimised contains the distances between the available incomplete data vector and the predicted vector. The non-negative *basis matrix* \mathbf{W} is assumed to be known from the available non-negative data matrix ${}_r\mathbf{S}$. The coefficient vector \mathbf{H}^+ is obtained considering the non-negativity constraint by solving the *non-negative least squares* problem

$${}_r\mathbf{M} \cdot \mathbf{H}^+ = {}_r\mathbf{R}, \quad (13)$$

with

$$\begin{aligned} {}_r\mathbf{M} &= (\mathbf{W}^T, \mathbf{W}) \\ {}_r\mathbf{R} &= (\mathbf{W}^T, \mathbf{S}^+) \end{aligned} \quad (14)$$

The non-negative constrained least squares problem in Eq. (13) is solved by an algorithm introduced in (VanBenthem and Keenan, 2004). Finally, replacing the missing elements in the incomplete vector of radiuses, the complete or repaired radiuses vector of the system response is reconstructed.

5.3.2. Upper-lower-bounds representation

For the upper-lower-bounds representation, the unconstrained GPOD and a constrained GPOD techniques are utilized to predict the upper and lower bounds respectively. The unconstrained GPOD described in the previous section can be applied for the prediction of either the upper bound or the lower bound of the interval surface settlement field. In this paper, the upper bound ${}_u\mathbf{S}$ is chosen to predict first and the lower bound ${}_l\mathbf{S}$ is approximated considering the predicted result of upper bound as a constraint in the reconstruction procedure.

5.3.3. Constrained GPOD

In particular, the intermediate solution ${}_l\hat{\mathbf{A}}$ of the *least squares* problem in Eq. (10) needs to satisfy a constraint as following

$${}_l\tilde{\mathbf{S}} \approx \hat{\Phi} \cdot {}_l\hat{\mathbf{A}} \leq {}_u\mathbf{S}. \quad (15)$$

This is done by implementing a quadratic programming algorithm, which uses an active set method similar to that introduced in (Gill et al., 1981).

6. Examples

6.1. VERIFICATION EXAMPLE

The proposed method for interval data is firstly illustrated with a benchmark from structural analysis. Figure 1 shows the chosen example, which is a cantilever beam with a moving single load. In this example, the interval bounds of the deflection $\bar{\mathbf{S}}$ and the modulus elasticity of the beam

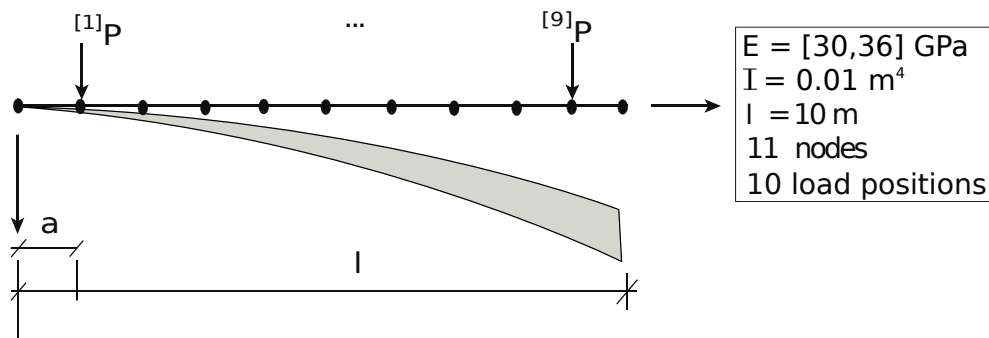


Figure 1. Verification example.

material $\bar{E} = [30, 36]$ GPa are the outputs and inputs of the investigations. The single load ${}^{[n]}P$ is considered as a time-variant parameter moving along the beam from node 2 to node 11. The scenarios of changing ${}^{[n]}P$ in each time step can be arbitrary but the value of ${}^{[n]}P$ is assumed to be restricted in a range from 10kN to 100kN. Given a scenario for stepwise moving load ${}^{[n]}P$ from $\mathbf{a}=1,2,\dots,9$ m, see Figure 2, the objective of this investigation is to predict the interval deflection of the complete beam when \mathbf{P}_t moves to the final position node 11, i.e. $\mathbf{a}=10$ m. This is done with the assumption such that only the interval deflection at nodes 2,6 and 10 (i.e. $\mathbf{x}=1,5$ and 9 m) can be

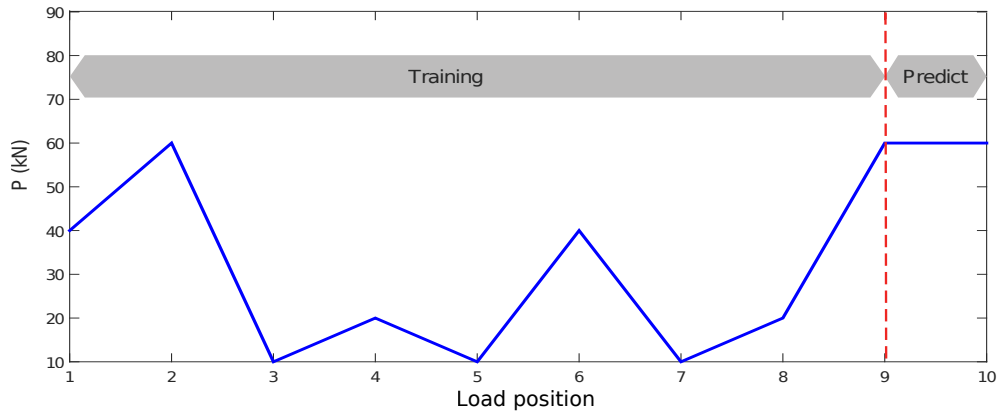


Figure 2. An arbitrary scenario of changing and moving load $^{[n]}P$.

observed. The proposed surrogate model predicts the deflections at other nodes of the beam. The predicted results are compared with the analytical solution given as

$$\bar{S} = \frac{Px^2}{6\bar{EI}}(3l - x), \text{ for } 0 < x < a, \quad (16)$$

$$\bar{S} = \frac{Pl^2}{6\bar{EI}}(3x - l), \text{ for } a < x < l. \quad (17)$$

In general, the interval bounds of the deflections for all beam nodes from step 1 to 9 can be calculated using a deterministic surrogate model with an optimization approach. However, in this example, the bounds $\bar{\mathbf{S}}$ can be obtained directly from the above equations using interval arithmetic. The verification procedure is done through the following steps:

1. The surrogate model is created based on results from 1600 snapshots which are obtained from combining 8 different intervals of \bar{E} and 200 scenarios of moving $^{[n]}P$. Each snapshot contains the interval displacements of 11 nodes of the beam from step 1 to 9. The snapshots data set is divided into sets for midpoints and radiuses as introduced previously.
2. The interval deflections of complete beam nodes from step 1 to 9 corresponding to the given interval of $\bar{E} = [30, 36]GPa$ and the scenario of changing $^{[n]}P$ from step 1 to 9, see Figure 2 are initialized by the POD-RBF approach. These results are represented by two matrices ${}_m\mathbf{S}$ and

${}_r\mathbf{S}$ in the types of midpoints and radiuses respectively.

$${}_m\mathbf{S} = \begin{bmatrix} 0.000 & 0.000 & 0.000 & 0.000 & 0.000 & 0.000 & 0.000 & 0.000 & 0.000 \\ 0.017 & 0.162 & 0.037 & 0.108 & 0.066 & 0.365 & 0.090 & 0.239 & 0.855 \\ 0.042 & 0.519 & 0.130 & 0.394 & 0.243 & 1.375 & 0.341 & 0.915 & 3.289 \\ 0.067 & 0.908 & 0.251 & 0.799 & 0.506 & 2.900 & 0.727 & 1.966 & 7.105 \\ 0.092 & 1.297 & 0.377 & 1.262 & 0.824 & 4.811 & 1.221 & 3.329 & 12.104 \\ 0.117 & 1.687 & 0.502 & 1.735 & 1.170 & 6.981 & 1.796 & 4.941 & 18.091 \\ 0.142 & 2.076 & 0.628 & 2.209 & 1.522 & 9.279 & 2.425 & 6.741 & 24.867 \\ 0.167 & 2.465 & 0.753 & 2.682 & 1.873 & 11.599 & 3.080 & 8.665 & 32.235 \\ 0.192 & 2.854 & 0.879 & 3.155 & 2.224 & 13.918 & 3.740 & 10.652 & 39.997 \\ 0.217 & 3.243 & 1.004 & 3.629 & 2.575 & 16.238 & 4.400 & 12.649 & 47.957 \\ 0.242 & 3.632 & 1.130 & 4.102 & 2.926 & 18.558 & 5.060 & 14.646 & 55.950 \end{bmatrix}$$

$${}_r\mathbf{S} = \begin{bmatrix} 0.000 & 0.000 & 0.000 & 0.000 & 0.000 & 0.000 & 0.000 & 0.000 & 0.000 \\ 0.003 & 0.015 & 0.008 & 0.015 & 0.015 & 0.039 & 0.020 & 0.035 & 0.082 \\ 0.008 & 0.050 & 0.027 & 0.056 & 0.056 & 0.147 & 0.075 & 0.133 & 0.315 \\ 0.013 & 0.087 & 0.053 & 0.114 & 0.116 & 0.309 & 0.161 & 0.286 & 0.680 \\ 0.018 & 0.124 & 0.079 & 0.180 & 0.189 & 0.513 & 0.270 & 0.485 & 1.159 \\ 0.023 & 0.161 & 0.106 & 0.247 & 0.268 & 0.744 & 0.396 & 0.720 & 1.732 \\ 0.028 & 0.198 & 0.132 & 0.315 & 0.349 & 0.989 & 0.535 & 0.982 & 2.381 \\ 0.033 & 0.235 & 0.158 & 0.382 & 0.429 & 1.237 & 0.680 & 1.262 & 3.086 \\ 0.038 & 0.272 & 0.185 & 0.449 & 0.510 & 1.484 & 0.826 & 1.552 & 3.830 \\ 0.043 & 0.309 & 0.211 & 0.517 & 0.590 & 1.731 & 0.971 & 1.843 & 4.592 \\ 0.048 & 0.347 & 0.238 & 0.584 & 0.671 & 1.979 & 1.117 & 2.133 & 5.357 \end{bmatrix}$$

The upper and lower bounds of the interval deflection field are computed as ${}_u\mathbf{S} = {}_m\mathbf{S} + {}_r\mathbf{S}$ and ${}_l\mathbf{S} = {}_m\mathbf{S} - {}_r\mathbf{S}$. The errors between the predicted bounds and analytical solutions, which are defined as following

$$error = \sqrt{\frac{\sum_{i=1}^N (\mathbf{S}_{approx}^i - \mathbf{S}_{analytical}^i)^2}{\sum_{i=1}^N (\mathbf{S}_{analytical}^i)^2}} \times 100\%, \quad (18)$$

are 5.0% and 5.3% for the upper bound and the lower bound, respectively.

- Finding the reduced bases of the matrices ${}_m\mathbf{S}$, ${}_r\mathbf{S}$, ${}_u\mathbf{S}$ and ${}_l\mathbf{S}$. The POD procedure are performed to obtain ${}_m\hat{\Phi}$, ${}_u\hat{\Phi}$ and ${}_l\hat{\Phi}$ for the midpoint, upper bound and lower bound matrices, respectively.

Whereas the NNMF approach is used to extract the reduced bases \mathbf{W} for $r\mathbf{S}$.

$$\begin{array}{c}
 \begin{bmatrix} 0.000 & 0.000 \\ 0.009 & 0.053 \\ 0.034 & 0.173 \\ 0.073 & 0.302 \\ 0.125 & 0.406 \\ 0.188 & 0.452 \\ 0.258 & 0.411 \\ 0.336 & 0.266 \\ 0.417 & 0.046 \\ 0.500 & -0.209 \\ 0.583 & -0.470 \end{bmatrix} \\
 {}_m\hat{\Phi} =
 \end{array}
 \quad
 \mathbf{W} =
 \quad
 \begin{array}{c}
 \begin{bmatrix} 0.000 & 0.000 \\ 0.009 & 0.020 \\ 0.034 & 0.079 \\ 0.074 & 0.168 \\ 0.126 & 0.269 \\ 0.188 & 0.360 \\ 0.259 & 0.419 \\ 0.336 & 0.433 \\ 0.417 & 0.410 \\ 0.499 & 0.365 \\ 0.582 & 0.316 \end{bmatrix} \\
 {}_u\hat{\Phi} =
 \end{array}
 \quad
 \begin{array}{c}
 \begin{bmatrix} 0.000 & 0.000 \\ 0.009 & 0.052 \\ 0.033 & 0.170 \\ 0.073 & 0.300 \\ 0.125 & 0.405 \\ 0.187 & 0.452 \\ 0.258 & 0.413 \\ 0.335 & 0.267 \\ 0.417 & 0.047 \\ 0.500 & -0.209 \\ 0.583 & -0.471 \end{bmatrix} \\
 {}_l\hat{\Phi} =
 \end{array}
 \quad
 \begin{array}{c}
 \begin{bmatrix} 0.000 & 0.000 \\ 0.009 & 0.054 \\ 0.034 & 0.175 \\ 0.073 & 0.305 \\ 0.125 & 0.407 \\ 0.188 & 0.451 \\ 0.259 & 0.410 \\ 0.336 & 0.265 \\ 0.417 & 0.046 \\ 0.500 & -0.209 \\ 0.583 & -0.469 \end{bmatrix}
 \end{array}$$

- The patterns of input-output data at nodes 2, 6 and 10 of the beam are utilized for constructing two separate RNNs to predict the midpoints and the radiuses for the interval deflections at these selected nodes. With an arbitrary input scenario of changing the load \mathbf{P}_t , the outputs, i.e. the deflections at 3 selected nodes, are computed from these RNNs. A network structure with one hidden layer containing 7 hidden neurons was sufficient to predict the midpoint. On the other hand, the radius prediction requires a two hidden layers RNN with 7 neurons per layer. In both networks, a delay of one time step has been selected for the context neurons. From the midpoint-radius prediction results, the upper and lower bounds of the three selected nodes ${}_u\bar{\mathbf{S}}_{RNN}$ and ${}_l\bar{\mathbf{S}}_{RNN}$ are calculated.

$${}_u\bar{\mathbf{S}}_{RNN} = \begin{bmatrix} 0.959 \\ 21.013 \\ 57.000 \end{bmatrix} \quad
 {}_u\bar{\mathbf{S}}_{an} = \begin{bmatrix} 0.967 \\ 20.833 \\ 56.700 \end{bmatrix} \quad
 {}_l\bar{\mathbf{S}}_{RNN} = \begin{bmatrix} 0.800 \\ 17.607 \\ 47.730 \end{bmatrix} \quad
 {}_l\bar{\mathbf{S}}_{an} = \begin{bmatrix} 0.806 \\ 17.361 \\ 47.250 \end{bmatrix}$$

The errors following Eq. (18) for upper and lower bounds approximation are 0.58% and 1.07%, respectively.

- Finally, the intervals of deflections of all 11 beam nodes in step 10 are predicted. The reduced bases ${}_m\hat{\Phi}$, \mathbf{W} , ${}_u\hat{\Phi}$ and ${}_l\hat{\Phi}$ are the inputs of the procedure together with the incomplete vectors ${}_m\mathbf{S}^*$, ${}_r\mathbf{S}^*$, ${}_u\mathbf{S}^*$ and ${}_l\mathbf{S}^*$. The outputs are the complete vectors ${}_{mr}\bar{\mathbf{S}}^*$ and ${}_{ul}\bar{\mathbf{S}}^*$ corresponding to midpoint-radius and upper-lower-bounds approaches. These two vectors are compared with reference analytical solution to verify the accuracy and effectiveness of the two methods.

As introduced previously, the computation of deflection intervals for the cantilever beam is carried out with two approaches: midpoint-radius (mid-rad) and upper-lower-bounds (up-low). The

Real-Time Prediction of Structural Processes with Polymorphic Uncertain Data

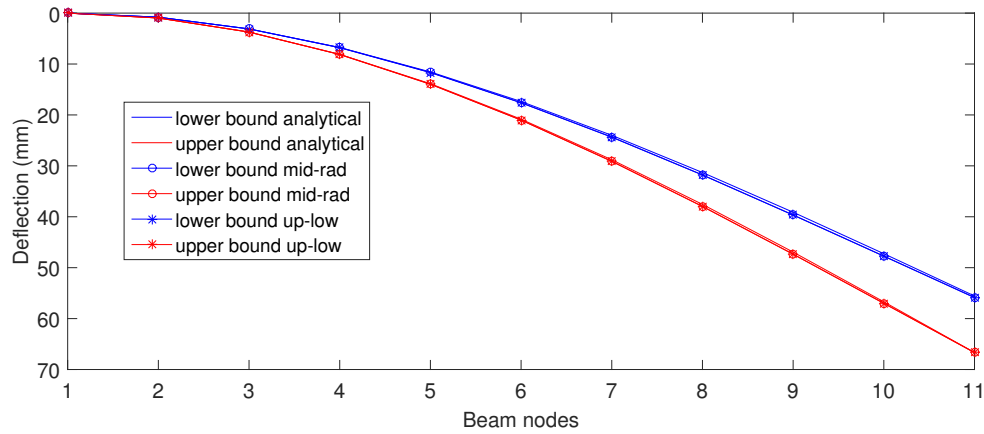


Figure 3. Comparison of predictions from two approaches (mid-rad and up-low) with the analytical solution.

final prediction results of the deflections at step 10 for $^{[10]}P = 60$ kN are

$$\begin{aligned}
 {}_{mr}\bar{\mathbf{S}}^* &= \begin{bmatrix} [0.000, 0.000] \\ \mathbf{[0.800, 0.959]} \\ [2.989, 3.838] \\ [6.657, 8.254] \\ [11.590, 14.047] \\ \mathbf{[17.607, 21.013]} \\ [24.422, 29.043] \\ [31.874, 37.882] \\ [39.718, 47.289] \\ \mathbf{[47.730, 57.000]} \\ [55.804, 66.725] \end{bmatrix} &
 {}_{ul}\bar{\mathbf{S}}^* &= \begin{bmatrix} [0.000, 0.000] \\ \mathbf{[0.800, 0.959]} \\ [3.112, 3.715] \\ [6.798, 8.113] \\ [11.689, 13.949] \\ \mathbf{[17.607, 21.013]} \\ [24.373, 29.093] \\ [31.800, 37.960] \\ [39.655, 47.352] \\ \mathbf{[47.730, 57.000]} \\ [55.840, 66.689] \end{bmatrix} &
 \bar{\mathbf{S}}^*_{analytical} &= \begin{bmatrix} [0.000, 0.000] \\ \mathbf{[0.806, 0.967]} \\ [3.111, 3.733] \\ [6.750, 8.100] \\ [11.556, 13.867] \\ \mathbf{[17.361, 20.833]} \\ [24.000, 28.800] \\ [31.306, 37.567] \\ [39.111, 46.933] \\ \mathbf{[47.250, 56.700]} \\ [55.556, 66.667] \end{bmatrix}
 \end{aligned}$$

Figure 3 illustrates the comparison of predictions using two representation approaches together with analytical solution. It is shown, that both methods provide very good predictions for the upper and lower bounds of beam deflection with errors of 0.61%, 1.18% from midpoint-radius representation and 0.34%, 1.09% for upper-lower-bounds representation, respectively. In addition, the prediction accuracy of the surrogate model is further validated by comparing 100 random validation cases with the analytical results. The average error of all validation cases is around 1% or less for both bounds and both methods, which proves the prediction capability of the surrogate model. Therefore the generated surrogate model will be further applied to the analysis considering polymorphic uncertain data, e.g. with in p-box approach. Here, the interval of \bar{E} is fixed in the range from 30 GPa to 36 GPa, meanwhile the moving $^{[n]}P$ scenario is treated as a stochastic process. 1000 samples of moving $^{[n]}P$ scenarios are randomly generated with the assumption that it follows a Gaussian distributed process with a mean value of $^{[n]}P = 50$ kN and the standard deviation of $\sigma = 15$ kN. Figure 4 depicts two curves, which are the minimum and maximum cdfs of the deflection of the beam at node 11 for time step 10, respectively. With the new surrogate model, the results of this analysis are obtained in only half an hour. This is a significant reduction in computation time comparing

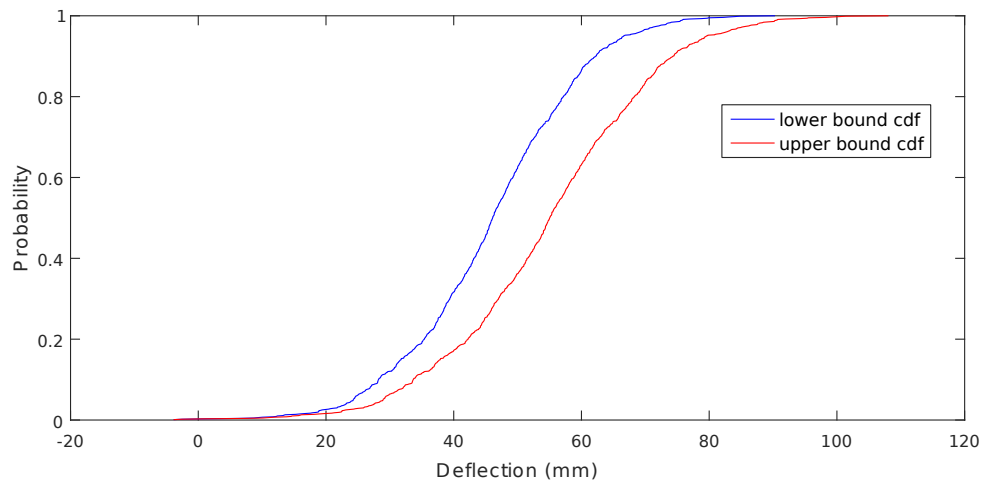


Figure 4. P-box for the deflection of the beam at node 11 for time step 10.

to the optimization approach which normally takes 10 hours to complete the analysis. This enables the application of more advanced and complicated reliability analysis in engineering problems.

6.2. APPLICATION EXAMPLE IN MECHANIZED TUNNELING

This section presents an application of the proposed surrogate modeling strategy for interval data based on a synthetic example representing a mechanized tunneling process. The interval results, which are computed from two representation approaches (mid-rad and up-low) are compared with the reference solution obtained from an optimization approach shown in (Freitag et al., 2015) in terms of prediction performance and computation time. The deterministic surrogate model is firstly trained with numerical results from FE simulation model `ekate` described in Section 2. The capability of the deterministic surrogate model is given with more details in (Freitag et al., 2015). Consequently, the interval analyses with the optimization approach are performed to generate data for the training of the proposed hybrid surrogate model with interval data to deliver predictions for the interval bounds of the surface settlements in further time steps of the tunneling process.

The synthetic example simulating the construction by a tunnel boring machine (TBM) of a tunnel section with 8.5m diameter and 8.5m overburden is generated using the `ekate` model. Figure 5 shows the simulation model with dimensions of 48m, 170m and 56m (in x,y,z directions, respectively). The length of each excavation step is 1.5m, i.e the tunnel section consists of 32 steps. The effect of two existing buildings to the surface displacement field is taken into account by applying substitute models with equivalent thickness of 5m and a stiffness of 50 GPa as shown in Figures 5. The tunnel construction process is modeled via a step-by-step procedure consisting of individual phases: soil excavation, applying support pressure, moving shield, applying grouting pressure and lining installation.

The tunnel is completely excavated through soil layer 1 of a ground model comprising of two parallel soil layers with different thicknesses and properties, see Figure 5. The groundwater table

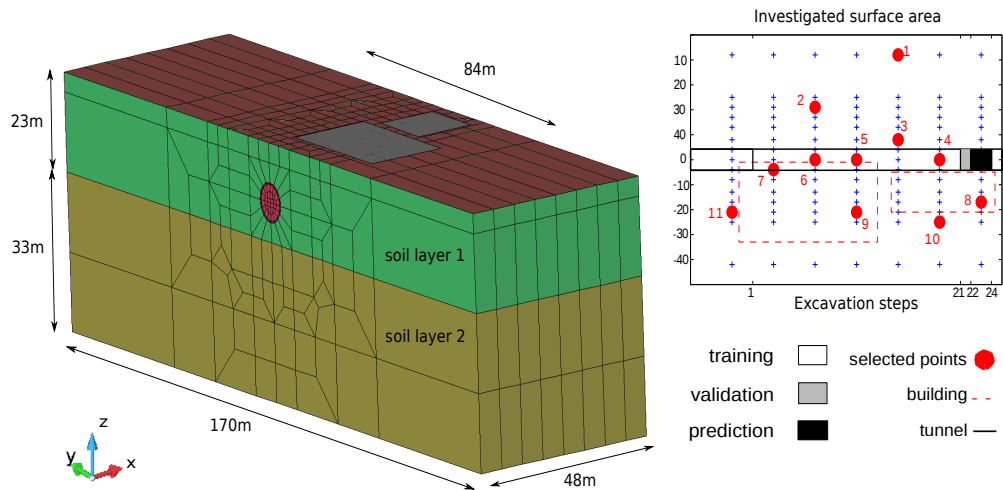


Figure 5. Numerical simulation model of a tunnel section (left) and investigates surface area (right).

is constant along the tunnel and at the ground surface. A time constant support pressure of 180 kPa is applied at the heading face. The grouting pressure $^{[n]}P$ in the tail void is considered with a particular value in each excavation step. The soil behavior is described by an elastoplastic model using Drucker-Prager yield criterion with a linear isotropic hardening. Linear elastic behavior is assumed for the shield and tunnel lining.

In this study, the elastic modulus E_1 of the first soil layer is taken as an uncertain parameter defined by an interval as $E_1 = [45,52]$ MPa to be comparable with the reference result in (Freitag et al., 2015). The grouting pressure $^{[n]}P$ in each excavation step n is chosen as varying operational parameter. The investigated ranges of these parameters are 20 to 110 MPa for E_1 and 130 to 230 kPa for $^{[n]}P$. It is assumed that the current state of the TBM advance corresponds to the 22nd step of the process, i.e. $n = 1, 2, \dots, 22$. The proposed surrogate model is utilized to predict the complete settlement fields in time step 23. Based on the calculated surface displacements, only an effective surface area of 42 m in y-direction from tunnel axis is investigated due to the fact, that the displacements of points located further than this distance are almost zero. Figure 5 (right) shows the investigated surface area with 105 points for which the Z-displacements are considered as outputs of the proposed method. In the example, the interval settlements of 11 selected monitoring points among 105 surface points are predicted by the RNNs with the approach of midpoint-radius representation. Whereas, the complete surface field is reconstructed with both mid-rad and up-low approaches.

Firstly, in the offline stage, 60 numerical simulations are performed to generate data for building the deterministic surrogate model based on a combination of 10 particular values of E_1 with 6 scenarios of changing $^{[n]}P$ from time step 1 to n . Then, possible intervals of E_1 are selected and an optimization based interval analysis is performed. The result of this interval analysis are used to generate the proposed surrogate model. Now, in the online stage, the interval surface settlement fields corresponding to the given interval of $E_1 = [45,52]$ MPa is computed in real-time.

Table V presents the relative error in percentage for the upper and lower bounds from both methods comparing to the reference solution in (Freitag et al., 2015). The errors are calculated by

$$error = \sqrt{\frac{\sum_{i=1}^N (\mathbf{S}_i^{opt} - \mathbf{S}_i^*)^2}{\sum_{i=1}^N (\mathbf{S}_i^{opt})^2}} \times 100\% , \quad (19)$$

Table V. Relative prediction error for the two approaches.

Error [%]	Upper bound		Lower bound	
	mid-rad	up-low	mid-rad	up-low
	8.9	8.0	6.2	5.9

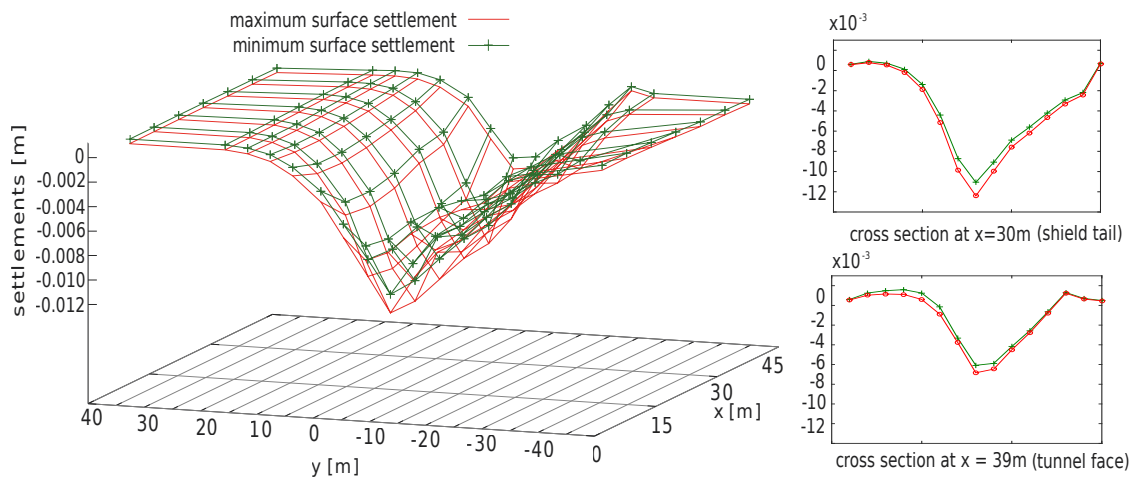


Figure 6. Typical interval field of tunneling induced surface settlements with $\bar{E}_1 = [45, 52]$ MPa.

In Figure 6, the typical computed interval settlement field is represented by its lower and upper bounds. The most important benefit of the proposed approach is, that the computation time is significantly reduced compared to the optimization approach. To obtain the interval bounds from the optimization approach, the required computation time is around 1.5 hours. The proposed approaches needs only 2 seconds to predict the interval settlement field with similar accuracy.

7. Conclusion

In the paper, a hybrid surrogate modeling strategy based on RNN and POD approaches has been developed to predict interval time variant settlement fields induced by mechanized tunneling taking uncertain geotechnical parameters quantified as intervals into account. In order to achieve real-time prediction capabilities, the hybrid RNN-GPOD surrogate model for deterministic data, which has

been previously developed by the authors, has been extended to process interval data by means of the midpoint-radius and upper-lower-bounds representations. Generally, both approaches produced very good prediction in comparison to the optimization approach for interval analysis. However, the computational time is significantly reduced from 1.5 hours by the optimization approach to 2 seconds by the proposed strategy. With such a fast response, it enables to quickly investigate the consequences of certain process parameters on the expected settlements in the subsequent excavation stages. Hence, the proposed strategy can be applied for real-time predictions to support the machine driver in steering the TBM. The upper-lower-bounds approach will be extended for fuzzy data. It is also planned to further develop a p-box approach for real-time applications.

Acknowledgements

Financial support was provided by the German Science Foundation (DFG) in the framework of project C1 of the Collaborative Research Center SFB 837 "Interaction Modeling in Mechanized Tunneling". This support is gratefully acknowledged.

References

- Beer, M., Y. Zhang, S. Quek and K. Phoon. Reliability Analysis with Scarce Information: Comparing Alternative Approaches in a Geotechnical Engineering Context. *Structural Safety*, 41:1–10, 2013.
- Bieniawski, Z. *Engineering Rock Mass Classifications*. Wiley, New York, 1989.
- Bui-Thanh, T., K. Damodaran and K. Willcox. Aerodynamic Data Reconstruction and Inverse Design using Proper Orthogonal Decomposition. *The American Institute of Aeronautics and Astronautics (AIAA)*, 42:1505–1516, 2011.
- Cao, B. T., S. Freitag and G. Meschke. A hybrid RNN-GPOD Surrogate Model for Real-time Settlement Predictions in Mechanised Tunnelling. *Advanced Modeling and Simulation in Engineering Sciences*, 3:Paper 5, 2016.
- Everson, R. and L. Sirovich. Karhunen-Loeve Procedure for Gappy Data. *Journal of the Optical Society of America A: Optics, Image Science and Vision*, 12(8):1657–1664, 1995.
- Ferson, S., V. Kreinovich, L. Ginzburg, D. S. Myers and K. Sentz. *Constructing probability boxes and Dempster-Shafer structures*. Tech. Rep. SAND2002-4015, Sandia National Laboratories, 2003.
- Fetz, T., M. Oberguggenberger, J. Jäger, D. Köll, G. Krenn, H. Lessmann and R. Stark. Fuzzy Models in Geotechnical Engineering and Construction Management. *Computer-Aided Civil and Infrastructure Eng.*, 14:93–106, 1999.
- Freitag, S. *Modellfreie numerische Prognosemethoden zur Tragwerksanalyse*, Dissertation, Veröffentlichungen – Institut für Statik und Dynamik der Tragwerke, Heft 19, TU Dresden, 2010.
- Freitag, S. Artificial Neural Networks in Structural Mechanics, in Y. Tsompanakis, J. Kruis, B. Topping (Editors), *Computational Technology Reviews*, Volume 12, pages 1–26. Saxe-Coburg Publications, Stirlingshire, 2015.
- Freitag, S., B. T. Cao, J. Ninić and G. Meschke. Hybrid Surrogate Modelling for Mechanised Tunnelling Simulations with Uncertain Data. *International Journal of Reliability and Safety*, 9(2/3):154–173, 2015.
- Freitag, S., B. T. Cao, J. Ninić and G. Meschke. Recurrent Neural Networks and Proper Orthogonal Decomposition with Interval Data for Real-Time Predictions of Mechanised Tunnelling Processes, *Computers and Structures*, 2016, submitted.
- Freitag, S., W. Graf and M. Kaliske. Recurrent Neural Networks for Fuzzy Data. *Integrated Computer-Aided Engineering*, 18(3):265–280, 2011.
- Freitag, S., R. L. Muhanna and W. Graf. Interval Monte Carlo simulation with neural network-based surrogate models. In: G. Deodatis, B. R. Ellingwood, D. M. Frangopol (eds.) *Safety, Reliability, Risk and Life-Cycle Performance of Structures and Infrastructures, Proceedings of 11th International Conference on Structural Safety and Reliability (ICOSSAR 2013)*, New York, Taylor and Francis, London, 431–438, 2013.

- Gill, P. E., W. Murray and M. Wright. *Practical Optimization*, Academic Press, London, 1981.
- Graf, W., M. Götz and M. Kaliske. Structural design with polymorphic uncertainty models. In: M. Modares (ed.) *Proceedings of the 6th Int. Conference on Reliable Engineering Computing (REC 2014)*, Chicago, 64–76, 2014.
- Hanss, M. The transformation method for the simulation and analysis of systems with uncertain parameters. *Fuzzy Sets and Systems*, 130(3):277–289, 2002.
- Hardy, R. L. Theory and Applications of the Multiquadric-biharmonic Method: 20 Years of Discovery 1968-1988. *Computers & Mathematics with Applications*, 19(8-9):163–208, 1990.
- Hotelling, H. Analysis of a Complex System of Statistical Variables into Principal Components. *Journal of Educational Psychology*, 24:417–441;498–520, 1933.
- Karhunen, K. Zur Spektraltheorie stochastischer Prozesse. *Annales Academiae Scientiarum Fennicae. Mathematica*, 34, 1946.
- Kasper, T. and G. Meschke. A 3D Finite Element Simulation Model for TBM Tunnelling in Soft Ground. *International Journal for Numerical and Analytical Methods in Geomechanics*, 28:1441–1460, 2004.
- Kim, H. and H. Park. Nonnegative Matrix Factorization Based on Alternating Nonnegativity Constrained Least Squares and Active Set Method. *SIAM Journal on Matrix Analysis and Applications*, 30(2):713–730, 2008.
- Laursen, T. *Computational Contact and Impact Mechanics*. Springer, Berlin-Heidelberg, 2002.
- Loeve, M. *Probability Theory II*, Volume 46 of *Graduate Texts in Mathematics*. Springer Verlag, New York, 1978.
- Lorenz, E. N. *Empirical Orthogonal Functions and Statistical Weather Prediction*, Technical Report 1, M.I.T, Department of Meteorology, 1956.
- Meschke, G. Consideration of Aging of Shotcrete in the Context of a 3D Viscoplastic Material Model. *International Journal for Numerical Methods in Engineering*, 39:3123–3143, 1996.
- Meschke, G., J. Ninic, J. Stascheit and A. Alsahly. Parallelized Computational Modeling of Pile-Soil Interactions in Mechanized Tunneling. *Engineering Structures*, 47:35 – 44, 2013,
- Moens, D. and D. Vandepitte. A survey of non-probabilistic uncertainty treatment in finite element analysis. *Computer Methods in Applied Mechanics and Engineering*, 194:1527–1555, 2005.
- Moens, D. and M. Hanss. Non-probabilistic finite element analysis for parametric uncertainty treatment in applied mechanics: Recent advances. *Finite Element Analysis and Design*, 47:4–16, 2011.
- Möller, B., W. Graf and M. Beer. Fuzzy Structural Analysis Using α -level Optimization. *Computational Mechanics*, 26:547–565, 2000.
- Möller, B. and M. Beer. Engineering Computation under Uncertainty – Capabilities of Non-traditional Models. *Computers and Structures*, 86:1024–1041, 2008.
- Moore, R. *Methods and Applications of Interval Analysis*, Volume 2. SIAM, Studies in Applied Mathematics, Philadelphia, 1979.
- Muhanna, R. L., H. Zhang, and R. L. Mullen. Interval Finite Elements as a Basis for Generalized Models of Uncertainty in Engineering. *Reliable Computing*, 13(2):173–194, 2007.
- Nagel, F., J. Stascheit and G. Meschke. Process-oriented Numerical Simulation of Shield Tunneling in Soft Soils. *Geomechanics and Tunneling*, 3(3):268–282, 2010.
- Nagel, F. and G. Meschke. An Elasto-plastic Three Phase Model for Partially Saturated Soil for the Finite Element Simulation of Compressed Air Support in Tunneling. *International Journal for Numerical and Analytical Methods in Geomechanics*, 34:605–625, 2010.
- Ninić, J. *Computational Strategies for Predictions of the Soil-structure Interaction during Mechanized Tunneling*, PhD thesis, Institute for Structural Mechanics, Ruhr University Bochum, 2015.
- Paatero, P. and U. Tapper. Positive Matrix Factorization: A Nonnegative Factor Model with Optimal Utilization of Error Estimates of Data Values, *Environmetrics*, 5(2):111–126, 1994.
- Rao, M. V. R., R. L. Mullen, and R. L. Muhanna. A new interval finite element formulation with the same accuracy in primary and derived variables. *International Journal for Reliability and Safety*, 5(3/4):336–357, 2011.
- Van Benthem, M. and M. Keenan. Fast Algorithm for the Solution of Large-Scale Non-Negativity-Constrained Least Squares Problems, *Journal of Chemometrics*, 18:441–450, 2004.
- Zhang, H., R. Mullen and R. Muhanna, Interval Monte Carlo methods for structural reliability, *Structural Safety*, 32:183–190, 2010.